Chemistry Europe
European Chemical Societies Publishing

Relevance of π-Backbonding for the Reactivity of Electrophilic Anions $[B_{12}X_{11}]^-$ (X=F, Cl, Br, I, CN)

Martin Mayer,*[a] Markus Rohdenburg,[a, b] Sebastian Kawa,[a] Francine Horn,[a] Harald Knorke,[a] Carsten Jenne,[c] Ralf Tonner,[a] Knut R. Asmis,[a] and Jonas Warneke*[a, d]

Abstract: Electrophilic anions of type $[B_{12}X_{11}]^-$ posses a vacant positive boron binding site within the anion. In a comparatitve experimental and theoretical study, the reactivity of $[B_{12}X_{11}]^-$ with X=F, Cl, Br, I, CN is characterized towards different nucleophiles: (i) noble gases (NGs) as σ-donors and (ii) CO/N_2 as σ-donor-π-acceptors. Temperature-dependent formation of $[B_{12}X_{11}NG]^-$ indicates the enthalpy order (X=CN) > (X=Cl) ≈ (X=Br) > (X=I) ≈ (X=F) almost independent of the NG in good agreement with calculated trends. The observed order is explained by an interplay of the electron deficiency of the vacant boron site in $[B_{12}X_{11}]^-$ and steric effects. The binding of CO and N_2 to $[B_{12}X_{11}]^-$ is significantly stronger. The B3LYP 0 K attachment enthapies follow the order (X=F) > (X=CN) > (X=Cl) > (X=Br) > (X=I), in contrast to the NG series. The bonding motifs of $[B_{12}X_{11}CO]^-$ and $[B_{12}X_{11}N_2]^-$ were characterized using cryogenic ion trap vibrational spectroscopy by focusing on the CO and N_2 stretching frequencies ν_{CO} and ν_{N_2}, respectively. Observed shifts of ν_{CO} and ν_{N_2} are explained by an interplay between electrostatic effects (blue shift), due to the positive partial charge, and by π-backdonation (red shift). Energy decomposition analysis and analysis of natural orbitals for chemical valence support all conclusions based on the experimental results. This establishes a rational understanding of $[B_{12}X_{11}]^-$ reactivety dependent on the substituent X and provides first systematic data on π-backdonation from delocalized σ-electron systems of *closo*-borate anions.

Introduction

The fixation and activation of small unreactive molecules represents one of the outstanding challenges in contemporary chemical research. Highly reactive intermediates offer the opportunity to activate the most inert compounds,[1] however, they often lack selectivity in chemical reactions. Therefore, we explore the defined bond formation of inert compounds with highly reactive molecular ions generated in the gas phase with the goal to accumulate the products in the condensed phase using high-flux ion soft-landing methods.[2] A fundamental understanding of the binding properties of reactive ions is the key to control these reactions and to select the best suited ion for a particular bond activation/formation process. Recently, anions of exceptional reactivity have been identified: collision-induced dissociation (CID) of gaseous *closo*-dodecaborate dianions $[B_{12}X_{12}]^{2-}$ (X = halogen, CN) generates $[B_{12}X_{11}]^-$ anions, which are strongly electrophilic and bind the larger noble gases (NGs) spontaneously at room temperature.[3] The counterintuitive electrophilic behavior of the anions was traced back to a substantial positive partial charge on the vacant boron atom in $[B_{12}X_{11}]^-$. The substituent X influences the reactive side in several ways: (i) The electronic structure of the ion and the positive partial charge on the vacant boron atom are strongly dependent on X, (ii) a reaction partner, which binds to the vacant boron site, will necessarily interact with the five substituents of the neighboring boron atoms. Ideally, the choice of the substituent X represents a sensitive adjustable parameter that allows tuning the reactivity of $[B_{12}X_{11}]^-$. However, no systematic study on the influence of the substituent X on the reactivity of $[B_{12}X_{11}]^-$ ions exists so far.

The first investigated electrophilic anion was $[B_{12}Cl_{11}]^-$ which binds Kr and Xe at room temperature.[3b] The positive partial charge of the vacant boron site was experimentally verified by a strong blue shift of the CO stretching frequency ν_{CO} in $[B_{12}Cl_{11}CO]^-$ in comparison to unbound CO. ν_{CO} is often used as

[a] Dr. M. Mayer, Dr. M. Rohdenburg, S. Kawa, F. Horn, H. Knorke, Prof. Dr. R. Tonner, Prof. Dr. K. R. Asmis, Dr. J. Warneke
Wilhelm-Ostwald-Institut für Physikalische und Theoretische Chemie
Universität Leipzig
Linnéstraße 2, 04103 Leipzig (Germany)
E-mail: martin.mayer@uni-leipzig.de
jonas.warneke@uni-leipzig.de

[b] Dr. M. Rohdenburg
Institut für Angewandte und Physikalische Chemie
Universität Bremen
Leobener Str. 5, 28359 Bremen (Germany)

[c] Prof. Dr. C. Jenne
Anorganische Chemie
Fakultät für Mathematik und Naturwissenschaften
Bergische Universität Wuppertal
Gaußstr. 20, 42119 Wuppertal (Germany)

[d] Dr. J. Warneke
Leibniz Institute of Surface Engineering (IOM)
Sensoric Surfaces and Functional Interfaces
Permoserstraße 15, 04318 Leipzig (Germany)

Supporting information for this article is available on the WWW under https://doi.org/10.1002/chem.202100949

a sensitive probe, which provides information about the charge state of a binding site.[4] The $[B_{12}(CN)_{11}]^-$ anion even binds to the significantly less polarizable Ar at room temperature and shows an even stronger ν_{CO} blue shift.[3a] It also binds Ne up to 50 K.[5] In line with these findings, computational investigations predicted larger NG binding enthalpies for $[B_{12}(CN)_{11}]^-$ than for $[B_{12}Cl_{11}]^-$. A recent investigation showed that $[B_{12}Cl_{11}]^-$ and $[B_{12}Br_{11}]^-$ react in a qualitatively similar way with alkyl chains.[2a] Beside these insights, little is known about the influence of the substituent X on the reactivity of the electrophilic anions $[B_{12}X_{11}]^-$. Here, we use a combined experimental and computational approach to perform a systematic investigation of $[B_{12}X_{11}]^-$'s reactivity dependent on X (with X=F, Cl, Br, I and CN).

NGs (He to Xe) were used as representatives of almost "pure" σ-donors to the electrophilic site. Their binding to the different electrophilic anions was compared at various temperatures using mass spectrometry. Furthermore, binding of the π-system containing diatomic molecules CO and N_2 to the $[B_{12}X_{11}]^-$ ions was studied and the CO/NN stretching frequency was probed using gas phase infrared photodissociation spectroscopy (IRPD). The results were compared with computationally determined reaction enthalpies and vibrational frequency analysis. An energy decomposition analysis (EDA) was performed and natural orbitals of chemical valence (NOCV) methods give insights into the bonding motifs of the NG, CO, and N_2 binding to $[B_{12}X_{11}]^-$. This allows interpretation of the experimental results using common chemical concepts like π-backbonding. This classical concept needs – under consideration of the results presented herein – to be extended by the case of delocalized σ-electron systems of *closo*-borate anions donating into antibonding orbitals of π-acceptors.

Results and Discussion

Binding noble gases: Reactivity order towards σ-donors

The reactivity of $[B_{12}X_{11}]^-$ anions towards the NGs He to Xe was systematically probed. Since these ion-NG reactions have no substantial barrier (see Supporting Information, Figure S1), we expect that formation of the $[B_{12}X_{11}NG]^-$ anions is mainly determined by the thermodynamic stability of the B-NG bond which is reflected by the calculated 0 K attachment enthalpies (ΔH^0_{attach}) shown in Figure 1(b). In the present experiment, the collision energy between $[B_{12}X_{11}]^-$ and NG is redistributed over the vibrational degrees of freedom, generating a "hot" $[B_{12}X_{11}NG]^-$ anion, which can easily dissociate via cleavage of the comparatively weak B-NG bond. The NG-containing adduct is detected if the formed collision complex is sufficiently thermalized by collisions with background gas molecules. For a given thermalization efficiency of the background gas (same temperature and pressure), the survival probability of $[B_{12}X_{11}NG]^-$ is strongly dependent on the NG binding enthalpy. Therefore, the maximum temperature (T_{max}), at which NG adduct formation can be detected, may serve as an experimental measure for comparison with ΔH^0_{attach}. Note, the T_{max}-values

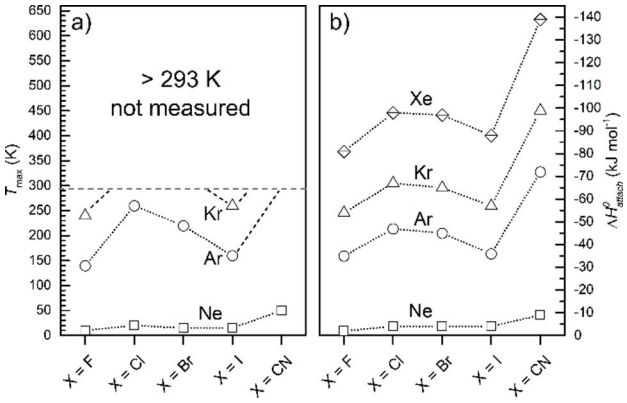

Figure 1. (a) T_{max} (in K) for $[B_{12}X_{11}NG]^-$ complexes for NG=Ne (squares), Ar (circles) and Kr (triangles). Experiments at temperatures > 293 K are not possible. T_{max} for all Xe adducts, the Kr adducts for X=Cl, Br, CN and the Ar adduct for X=CN is higher than 293 K. Dashed lines indicate the presumed trend for anion-NG complexes. The corresponding mass spectra, for the determination of T_{max}, are shown in the Supporting Information, Figures S2–S20. (b) ZPE- and BSSE-corrected ΔH^0_{attach} (in kJ mol^{-1}) of the Ne (squares), Ar (circles), Kr (triangles) and Xe (crossed out squares) complexes.

represent only a relative and qualitative measure for the trend within the series of tested ions.

The $[B_{12}X_{11}]^-$ anions were trapped with the collision gases He, Ne, Ar, Kr and Xe at different ion trap temperatures under otherwise equal conditions (see experimental section). The formation of $[B_{12}X_{11}NG]^-$ was determined (see Figure 1a) in the range between 6 K and 293 K. Even at the lowest possible temperature (6 K), we did not observe He adduct formation for all investigated anions. However, all $[B_{12}X_{11}]^-$ anions form stable adducts with Xe at 293 K. Moreover, $[B_{12}(CN)_{11}]^-$, $[B_{12}Cl_{11}]^-$, and $[B_{12}Br_{11}]^-$ also form stable compounds with Kr at 293 K, whereas Kr adduct formation for $[B_{12}I_{11}]^-$ and $[B_{12}F_{11}]^-$ is only observed up to 260 K and 240 K, respectively. Ar binding at 293 K is only observed for $[B_{12}(CN)_{11}]^-$ in accordance with Ref. [3a] while the other $[B_{12}X_{11}]^-$ anions still bind Ar in a temperature range from 140 (X=F) to 260 K (X=Cl). Ne adduct formation with the most electrophilic anion $[B_{12}(CN)_{11}]^-$, up to 50 K, was recently reported.[5] For the other anions, adduct formation is observed between 10 K ($[B_{12}F_{11}]^-$) and 20 K ($[B_{12}Cl_{11}]^-$). The T_{max}-curves for Kr, Ar and Ne reveal a seemingly NG-independent reactivity trend following the sequence (increasing reactivity): $[B_{12}F_{11}]^- \approx [B_{12}I_{11}]^- < [B_{12}Br_{11}]^- \approx [B_{12}Cl_{11}]^- \ll [B_{12}(CN)_{11}]^-$. The corresponding ΔH^0_{attach} are plotted in Figure 1b. All values are negative showing that the NG adduct formation is thermochemically favorable. The absolute values increase from Ne to Xe as expected. The trend in calculated values for ΔH^0_{attach} correlates well with the trend found for the experimentally determined T_{max} . The ability to bind noble gases is usually associated with a strong electrophilic character of the binding site. The calculated charges, obtained from natural population analysis (NPA), of the vacant boron atom in $[B_{12}X_{11}]^-$ are: (X=F, +0.45 *e*) < (X=Cl, +0.64 *e*) ≈ (X=Br, +0.64 *e*) ≈ (X=I, +0.66 *e*) < (X=CN, +0.82 *e*). However, the reduced reactivity of $[B_{12}I_{11}]^-$ in comparison to $[B_{12}Br_{11}]^-$ and $[B_{12}Cl_{11}]^-$ cannot be traced back to a reduced electrophilicity of the vacant boron atom.

Binding CO and N_2: The influence of π-acceptors

In contrast to the previously reported trends in ΔH^0_{attach} of the NG complexes, we find a different order for the respective CO/N_2 adducts, $[B_{12}X_{11}CO]^-$ and $[B_{12}X_{11}N_2]^-$: $[B_{12}I_{11}]^- < [B_{12}Br_{11}]^- < [B_{12}Cl_{11}]^- < [B_{12}(CN)_{11}]^- < [B_{12}F_{11}]^-$ (see Table 1). The comparatively weak NG binder $[B_{12}F_{11}]^-$ represents the strongest binder in the case of CO and N_2. For more insights, the stretching frequency ν_{CO} and ν_{N_2} of $[B_{12}X_{11}CO]^-$ and $[B_{12}X_{11}N_2]^-$ were investigated. Red shifts of ν_{CO} and ν_{N_2} are comprehensively discussed in the literature for transition metal (TM) complexes. The electrostatic effect of a negative binding partner can induce a red shift in both cases (see Supporting Information, Figure S21),[3b,4,6] but usually electron transfer from TM d-orbitals into CO and N_2 π*-orbitals (π-backbonding) is responsible for bond weakening and ν_{CO} and ν_{N_2} shift to lower frequencies with respect to the free CO and N_2 molecules.[7] Blue shifts of ν_{CO} were frequently discussed, when the binding partner is positively charged and π-backbonding has no or only small influence (e.g. non-classical carbonyl complexes).[8] The role of the TM←C σ-donation on this blue shift has been the subject of an intense debate in the literature.[4,6,9] In-depth theoretical studies have established that this σ-electron pair donation has no significant influence on ν_{CO}.[6,9b,10] Instead, ν_{CO} shifts are strongly influenced by electrostatic effects: the orbitals of the CO bond are polarized towards the oxygen atom and this polarization is reduced by the electric field of a positive charge in front of the C atom. The increased covalent character of the bond affects an increase of the force constant of the stretching vibration (blue shift). Therefore, CO has been established as a sensitive probe for the electrostatic situation at a binding site.[4,11] The response of this probe towards $[B_{12}X_{11}]^-$ is particularly interesting, because the CO molecule binds to a boron atom with positive partial charge, which is incorporated into an overall anionic framework. Although the N_2 stretching frequency responds qualitatively similar to electrostatics, experimental observations of ν_{N_2} blue shifts appear scarce. ν_{N_2} is significantly less influenced by electrostatics than ν_{CO}. Instead, orbital interactions have a much stronger influence and usually red shifts are observed. Blue shifts of ν_{N_2} have been theoretically predicted for highly electrophilic cations, which cannot weaken the N_2 triple bond by providing electron density (e.g. methyl cation $[CH_3]^+$).[12]

Figure 2a–e shows the IRPD spectra of CO-tagged $[B_{12}X_{11}CO]^-$ ions in the typical CO stretching frequency region (

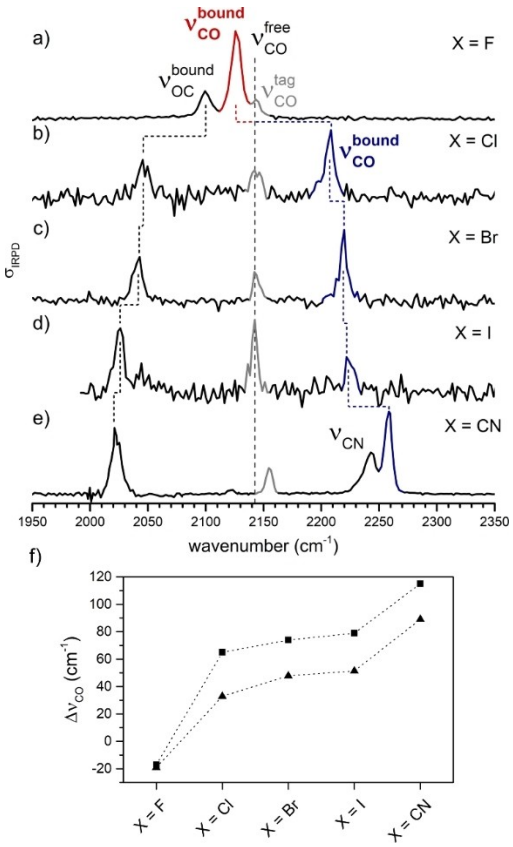

Figure 2. IRPD spectra of CO-tagged $[B_{12}X_{11}CO]^-$ ions in the spectral range from 1950 to 2350 cm^{-1}, with X=F (a), Cl (b), Br (c), I (d), CN (e). Bands are labeled and color-coded according to the respective frequency shift (red shift = red, blue shift = blue, for band assignment see Supporting Information, section S5). (f) Measured (black squares) and calculated (black triangles) stretching frequency shifts of carbon-bound CO (with respect to the experimentally determined/calculated free CO stretching). Calculated results for the ν_{OC} stretching vibration are discussed in the Supporting Information, section S6.

$\nu^{free}_{CO} = 2143\ cm^{-1}$).[7a] Three different CO absorptions can be distinguished in each individual spectrum resulting from three different binding motifs: One band originates from the CO molecules which bind with the carbon atom (ν_{CO}). The second band originates from oxygen-bound CO molecules (ν_{OC}). Qualitatively, the position of ν_{OC} develops oppositely to that of the C-bound CO along the series of investigated ions. A third band originates from a more loosely bound CO, which acts as a

Table 1. Calculated 0 K attachment enthalpies (in $kJ\,mol^{-1}$) for the reactions of $[B_{12}X_{11}]^-$ with CO, N_2 and Xe; B–C, B–N and B–Xe bond lengths in the optimized geometry and differences of C–O and N–N bond lengths (both in Å) in comparison to unbound CO/N_2.

Y\X	$[B_{12}X_{11}Y]^-$	F	Cl	Br	I	CN
CO	ΔH^0_{attach}	−267	−246	−239	−227	−252
	r(B–C)	1.466	1.491	1.502	1.513	1.519
	Δr(C–O)	+0.008	−0.001	−0.003	−0.004	−0.008
N_2	ΔH^0_{attach}	−166	−156	−150	−138	−165
	r(B–N)	1.444	1.467	1.475	1.484	1.495
	Δr(N–N)	+0.013	+0.005	+0.004	+0.003	+0.002
Xe	ΔH^0_{attach}	−81	−98	−97	−88	−139
	r(B–Xe)	2.297	2.286	2.293	2.316	2.271

messenger molecule (ν_{CO}^{tag}) and exhibits almost no shift compared to the free CO stretching frequency. In the spectrum of $[B_{12}(CN)_{11}CO]^-$ (Figure 2e) an additional band (ν_{CN}) appears at 2245 cm^{-1}, which originates from the stretching vibrations of the CN substituents as evidenced by labeling experiments.[3a] We focus our discussion in the following on the carbon-bound CO, since this binding motif is intensively discussed in the literature with respect to "charge probing" of the free binding site. A discussion of the oxygen-bound CO binding motive can be found in the Supporting Information, section S4. Figure 2f compares the experimentally found ν_{CO} values with the results of harmonic frequency analysis which show the same trend along the series of ions. Experimentally (and computationally) obtained blue shifts for X=Cl to I range from 65 cm^{-1} (33 cm^{-1}) to 79 cm^{-1} (51 cm^{-1}). The $[B_{12}(CN)_{11}CO]^-$ anion shows the largest blue shift of 115 cm^{-1} (89 cm^{-1}). In contrast, ν_{CO} in $[B_{12}F_{11}CO]^-$ exhibits a red shift of 17 cm^{-1} (19 cm^{-1}).

The IRPD spectra of all $[B_{12}X_{11}N_2]^-$ ions are shown in Figure 3. The measured ν_{N_2} frequencies for all halogenated clusters are red-shifted with respect to the stretching frequency of free N_2, ranging from 97 cm^{-1} for $[B_{12}F_{11}N_2]^-$ over 28 cm^{-1} for $[B_{12}Cl_{11}N_2]^-$, 17 cm^{-1} for $[B_{12}Br_{11}N_2]^-$ and 14 cm^{-1} for $[B_{12}I_{11}N_2]^-$, respectively. Only in the case of $[B_{12}(CN)_{11}N_2]^-$ a slight blue shift of +5 cm^{-1} is observed. The computationally predicted trend of the shifts is in good agreement with the experimentally observed trend, however, the values deviate by 51 to 33 cm^{-1}.

For detailed theoretical insights on the interaction between Xe, CO and N_2, EDA was performed.

Energy decomposition analysis (EDA)

Analysis of the bonding interaction between $[B_{12}X_{11}]^-$ and NG, CO or N_2 in terms of a decomposition of bonding contributions into orbital interaction, electrostatic interaction, dispersion attraction and Pauli repulsion by EDA is shown in Figure 4a–d. As an example for binding of the different NGs investigated, only the results for the Xe adducts are shown, the data for other NGs are available in the Supporting Information, section S7. Similar trends are found for N_2 and CO along the series of $[B_{12}X_{11}]^-$ ions although the absolute values for the individual energy components are larger for CO due to the stronger bond formed. Therefore, only the values for CO as a representative for a diatomic molecule with a π-donation capability are shown. The total interaction energies (see Supporting Information, Table S7) reproduce the trends found for the attachment

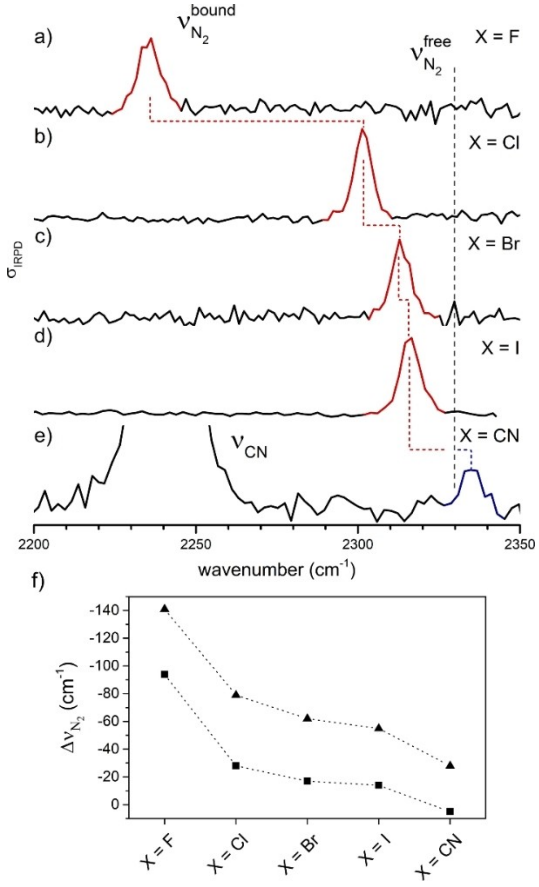

Figure 3. IRPD spectra of D_2-tagged $[B_{12}X_{11}N_2]^-$ ions for X=F–I and N_2 tagged $[B_{12}(CN)_{11}N_2]^-$ ions in the spectral range from 2200 to 2350 cm^{-1}, with (a) X=F, (b) X=Cl, (c) X=Br, (d) X=I, (e) X=CN (for band assignment see Supporting Information, section S5). (f) Measured (black squares) and calculated (black triangles) stretching frequency shifts of ν_{N_2} (with respect to the experimentally determined/calculated free N_2 stretching).

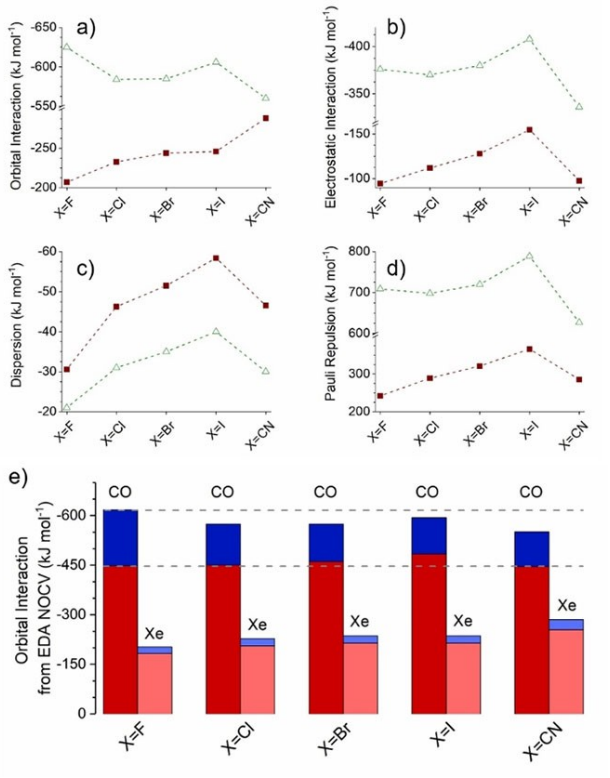

Figure 4. Results of the energy decomposition analysis for the binding of Xe (brown squares) and CO (green triangles): a) orbital interaction, b) electrostatic interaction, c) dispersion attraction and d) Pauli repulsion, e) partitioning of the orbital interaction into σ-type (red) and π-type contributions (blue) as derived from ETS-NOCV analysis. A comprehensive table of all EDA values can be found in the Supporting Information, section S7.

enthalpies at 0 K indicating that the deformation of the two moieties forming the bond are not decisive (small preparation energy). Therefore, quantitative differences to the previously discussed ΔH^0_{attach} are present but the trends along the series are clearly in agreement.

The EDA shows that orbital interaction is predominantly responsible for the stronger CO binding in the case of $[B_{12}F_{11}]^-$, which is a comparatively weak bonding partner for pure σ-donors like NGs (see Figure 4a). Further decomposition of the orbital interaction in terms of the Extended Transition State-Natural Orbitals for Chemical Valence (ETS-NOCV) method allows for a quantitative evaluation of σ-donation and π-back-donation (the terminology for σ- and π-type orbitals is used with respect to B–Ng/CO/N_2 bond axis. Strictly speaking, the point-group symmetry of the molecule does not allow this terminology). The four major deformation densities[13] derived from the ETS-NOCV analysis account for over 97% of the total orbital interaction energy. These deformation densities represent in all cases two σ -type NOCV pairs and two π-type NOCV pairs. The two π-type NOCV pairs have almost the same energetic contribution to the orbital interaction. A table with all values is given in the Supporting Information, section S8. Figure 4e visualizes the contribution of σ- and π-type deformation densities to the overall orbital interaction. This analysis shows that the comparatively strong binding of CO (and N_2, see Supporting Information, section S7) by $[B_{12}F_{11}]^-$ is based on a larger contribution of π-backbonding, which is not possible for NG. The small contribution of a π-type deformation density to Xe binding is mainly associated with polarization and π-donation from the NG to the B_{12} unit, see section S9 in the Supporting Information. The importance of this bonding motif is strongest for X=CN.

The visualization of the deformation density is used to demonstrate the charge transfer between the two fragments. Figure 5 shows the deformation density with the largest contribution of σ- and π-type for the $[B_{12}F_{11}]^-$ ion and the CO molecule. Similar representations for other combinations of $[B_{12}X_{11}]^-$ anions with CO and N_2 can be found in the Supporting Information, section S9. The deformation density (charge transfer from red to blue regions) depicts that the B–C σ-bond is formed by donation from the CO HOMO to the p-type orbital at the electrophilic vacant boron atom. In contrast, the second largest NOCV originates from charge transfer from the B_{12} unit to the CO orbitals of π-symmetry. The molecular orbitals (more specifically, the symmetrized fragment orbitals, SFOs[14]) with highest contribution to this NOCV can be clearly associated with the HOMO-1 orbital for X=F. A very similar picture was found for X=Cl and CN. In contrast, for X=Br and I the canonical orbitals associated with the SFOs of highest contribution to the π-backbonding are much lower in energy than the highest lying orbitals of the fragments. This demonstrates that a simple frontier orbital picture is insufficient for understanding the intrinsic ability for π-backbonding of $[B_{12}X_{11}]^-$ ions. For larger halogens (in particular for X=I) lone electron pairs of the halogen substituents constitute the HOMO[15] and do not participate in π-backbonding.

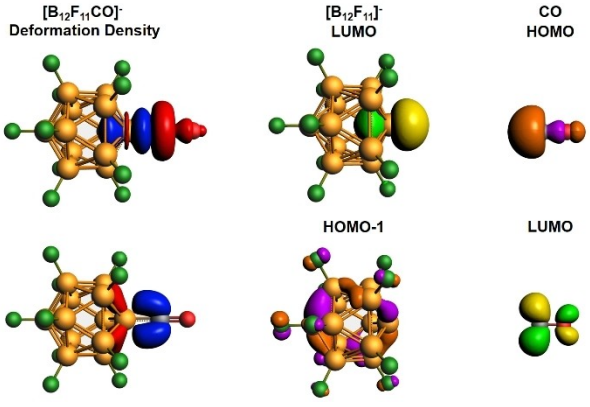

Figure 5. The deformation densities with the largest eigenvalues are shown on the left (isovalue 0.003 a.u.). Note that a second deformation density of π-type with an almost equal contribution to the orbital energy exists, as typical for π-type bonding motifs. Charge flow occurs from red to blue regions. The canonical frontier orbitals of $[B_{12}F_{11}]^-$ and CO are shown on the right – they are the major MO contributions to the deformation densities shown. Colors represent different signs of the wavefunction (isovalue 0.07 a.u.).

It cannot be disentangled from the EDA of the equilibrium adduct geometry if the comparatively larger orbital interaction for X=F results from stronger intrinsic electron donation properties, or if a shorter B–C bond length due to reduced steric hindrance (Pauli repulsion) is mainly responsible. It should be noted that orbital interactions usually increase with reduced bond length but π-type contributions have a stronger distance dependence than σ-type contributions. Therefore, we performed a "computational experiment" using ETS-NOCV decomposition of the orbital interaction for a fixed C–O bond length and various B–C distances. At the same B–C and C–O bond lengths, the calculated contribution from π-backbonding orbital interactions was always higher for X=F than for X=Cl, Br, I, CN, (see Supporting Information, section S10). This confirms that a higher intrinsic electron donation ability into π-bonds is present for X=F.

Discussion of observed trends

It may be assumed that the enthalpy of σ-bond formation between a nucleophile and $[B_{12}X_{11}]^-$ is directly related to the positive charge of the vacant boron site. However, although the vacant boron site for X=I is slightly more positive than for X=Br and Cl (shown by the analysis of ν_{CO} and NPA), the binding enthalpy for all NGs, CO and N_2 significantly decreases and the bond length increases (see Figure 1 and Table1). This effect may be attributed to the steric demand of iodine. The vacant boron site is surrounded by five substituents X, which interact with the binding partner. EDA analyses show that the attractive contributions (electrostatic, dispersion and orbital interactions) for X=I are larger than for X=Cl, Br but the increase in Pauli repulsion is even stronger, resulting in an overall smaller binding energy. This confirms that steric effects are responsible for the comparatively small binding enthalpies in the case of X=I in all cases. The trend of NG binding enthalpy compared

with the trend in CO/N_2 binding enthalpies (compare Figure 1 with Table 1) suggests that the π-bonds of the diatomic molecules are responsible for an additional interaction (beside the σ-bond) which is particularly strong in the case of X=F. Figure 5 underlines that the classical picture of σ-donor-π-acceptor interaction, is valid to describe their interaction with electrophilic anions. Although the effect is mainly known from TMs, electron transfer from occupied orbitals into the CO π*-orbitals has also been observed for main group atoms.[16] Also boron containing ions with π electron systems are known, which exhibit a red shift of ν_{CO} compared to unbound CO.[17] The potential influence of π-backbonding from the delocalized σ-electron system of *closo*-borate anions into antibonding orbitals of a substituent has not been discussed before in the literature. π-backdonation strengthens the interaction between $[B_{12}X_{11}]^-$ and CO/N_2, but weakens the corresponding CO and NN bonds. Simultaneously, the electrostatic effect of the vacant positive boron atom strengthens these bonds. However, the relative weight of these two counteracting effects is different for CO and N_2 as known, for example, for the corresponding complexes of the phenyl cation. ν_{CO} in $[C_6H_5CO]^+$ shows a substantial blue shift due to the positive carbon binding site, while ν_{N_2} is red-shifted in $[C_6H_5N_2]^+$,[12] due to electron donation into π*-orbitals from the π-system of the phenyl cation.

This establishes the following picture: The shift of the CO stretching frequency is determined by the electrostatic effect of the vacant positive boron atom rather than the overall negative charge of the anion. Only in the case of X=F, bond-weakening by π-backdonation overcompensates this effect. The red-shift of ν_{CO} cannot be explained by electrostatic effects alone (see Supporting Information, section S11 for a detailed discussion). In contrast, ν_{N_2} which is particularly sensitive to π-backdonation, shows a red shift for X=F–I. X=F exhibits the strongest effect. For X=CN the occupied orbitals responsible for backdonation are low in energy[3a] and contribute significant less to the bonding. The strong electrostatic effect of the vacant boron site overcompensates the weak π-backdonation, which results in a small blue shift. $[B_{12}F_{11}]^-$ is the strongest CO/N_2 binder followed by $[B_{12}(CN)_{11}]^-$, however, the bonding motif is very different. While strong binding to the latter is based on exceptional electron accepting properties (see NG binding), the strong CO and N_2 binding of the former is based on favorable back-donation properties.

Conclusion

The substituent X has a strong and complex influence on the reactivity of $[B_{12}X_{11}]^-$ anions. Reactivity rankings are furthermore strongly dependent on the reaction partner (here exemplified for CO/N_2 vs. NGs). Investigated differences in attachment enthalpies, the analysis of the CO and N_2 stretching frequencies and EDA of all adducts resulted in a comprehensive set of data which improves the understanding about the reactivity of $[B_{12}X_{11}]^-$ ions. In particular the important role of π-backbonding has been demonstrated. These insights may become valuable for selecting a particular electrophilic anion for tailored reactions with inert compounds. Electrophilic anions have already been proven to be valuable for direct reactions with saturated hydrocarbons,[2a] activation of CO and N_2 as demonstrated here, and might, for instance, allow for interesting chemistry with carbon dioxide, chlorofluorocarbon and other small but stable molecules. The obtained insights are also important to understand the binding motifs of boron-substituent bonds and their chemical properties also in the condensed phase.

Experimental Section

Mass spectrometry and gas phase vibrational spectroscopy

Mass spectrometric investigations of $[B_{12}X_{11}NG]^-$ and IRPD spectroscopy of CO-tagged $[B_{12}X_{11}CO]^-$, D_2-tagged $[B_{12}X_{11}N_2]^-$ and N_2-tagged $[B_{12}(CN)_{11}N_2]^-$ ions were performed using a 6 K ion trap triple mass spectrometer.[18] Briefly, $[B_{12}X_{11}]^-$ ions were produced in a nanospray ion source via skimmer collision-induced dissociation (sCID) of the precursor dianions $[B_{12}X_{12}]^{2-}$, which were synthesized by published procedures.[5,19] The ion beam was collimated and compressed in phase space in a He buffer-gas filled radio frequency (RF) ion-guide, held at room temperature. Anions of interest were then mass-selected using a quadrupole mass-filter and subsequently trapped in a buffer gas-filled RF ring-electrode ion-trap, which can be operated at temperatures between 6 K and room temperature. Collisions of the trapped ions with the buffer gas inside the ion guide provided gentle thermalization/cooling of the internal degrees of freedom close to desired temperature.

$[B_{12}X_{11}N_2]^-$ (for X=F, Cl, Br and I) complexes were formed in the RF ion guides filled with a 10% N_2 in He mixture . $[B_{12}X_{11}NG]^-$, $[B_{12}X_{11}CO]^-$ and $[B_{12}(CN)_{11}N_2]^-$ complexes were formed via three-body collisions[20] in the ion trap filled either with a 10% NG in He mixture, a 0.5% CO in He or a 10% N_2 in He mixture . The ion-trap temperature at which the signal of the $[B_{12}X_{11}NG]^-$ ions dropped below a signal to noise ratio of 3:1 served as maximum temperature of $[B_{12}X_{11}NG]^-$ complex formation (T_{max}). However, it should be noted that the absolute number shown by our temperature measurement should not be interpreted as the exact ion temperature: the internal temperature of captured ions under these conditions is typically estimated to be slightly higher which can be rationalized by absorption of infrared blackbody radiation, radio-frequency heating and inefficient energy transfer.[21] Furthermore, the exact temperature, which results in a diminishing $[B_{12}X_{11}NG]^-$ signal, depends on the ion trapping, ion transfer and detection efficiency and cannot be quantitatively compared even if the experiment is otherwise performed under same conditions.

Due to the high dissociation threshold of the $[B_{12}X_{11}CO]^-$ and $[B_{12}X_{11}N_2]^-$ ions, IR photodissociation under linear absorption conditions, which implies dissociation after the absorption of a single photon, was not possible. Therefore, an IRPD spectrum of the tagged complexes $[B_{12}X_{11}CO]^-\cdot CO$, $[B_{12}X_{11}N_2]^-\cdot(D_2)_n$ (for X=F, Cl, Br, I) and $[B_{12}(CN)_{11}N_2]^-\cdot N_2$ was recorded. Using the second, more loosely bound, gas molecule (CO, N_2 or D_2 respectively) as a tagging molecule reduces the dissociation threshold sufficiently to allow for photodissociation in the linear absorption regime. This approach has been applied to $[B_{12}X_{11}]^-$ anions previously.[3] According to our DFT calculations the tagging molecules have a negligible influence on the IRPD spectrum of $[B_{12}X_{11}CO/N_2]^-$. All anions were extracted from the ion trap after 100 ms, focused into the center of the extraction region of an orthogonally mounted reflectron time-of-flight (TOF) tandem photofragmentation mass-spectrometer, and

subsequently accelerated towards a microchannel plate detector. TOF mass spectra were recorded by averaging over 50-200 extraction cycles.

IRPD spectra were obtained by irradiating the ions in the center of the extraction region of the TOF mass spectrometer with an IR laser pulse from a Nd:YAG (Continuum Surelight EX1) pumped OPO/OPA/$AgGaSe_2$ laser system (Laser Vision)[22] operated at 10 Hz and with a bandwidth of approximately 3.5 cm^{-1}. IRPD spectra were recorded by continuously scanning the laser wavelength, which is monitored online (HighFinesse ES6-600 wavelength meter), with a scan speed such that a TOF mass spectrum averaged over 20 laser shots is obtained every 2 cm^{-1}. Typically, three to four scans are measured and averaged to obtain an IRPD spectrum. The photodissociation cross-section σ_{IRPD} is determined as described previously.[18]

Due to the natural abundance of two boron isotopes (80% ^{11}B, 20% ^{10}B), two chlorine isotopes (76% ^{35}Cl, 24% ^{37}Cl), and two bromine isotopes (51% ^{79}Br, 49% ^{81}Br) an isotopologue distribution is observed for each $[B_{12}X_{11}]^-$ ion in the mass spectrum. In order to improve the signal-to-noise ratio of the IRPD spectra the complete distribution (see mass spectra Supporting Information, section S2) was mass-selected for the IRPD measurements.

Computational details

Electronic structure calculations, vibrational frequency analysis, 0 K attachment enthalpy calculations and natural population analysis (NPA)[23] were carried out with the Gaussian 09, rev. D.01[24] and Gaussian 16, rev. C.01[25] software packages using the B3LYP functional[26] in combination with the Def2-QZVPP basis set,[27] applying dispersion-correction using Grimme's DFT-D3 model with Becke-Johnson damping.[28] The CO stretching frequency shifts were obtained from computed harmonic vibrational frequencies. In the special case of $[B_{12}F_{11}OC]^-$ also MP2/Def2-TZVPP optimization and frequency analysis was performed. Zero-point vibrational energy (ZPE) corrections were determined using harmonic frequency analysis. 0 K attachment enthalpies (ΔH^0_{attach}) were calculated as the differences between electronic energies of the product ($[B_{12}X_{11}Y]^-$) and the separated reagents ($[B_{12}X_{11}]^-$ and Y) with ZPE- and basis set superposition error (BSSE)-corrections. BSSE corrections were performed using the counterpoise method.[29] Energy decomposition analyses (EDAs)[14,30] were performed with the Amsterdam Density Functional (ADF) software package (version r68924 from 2018)[30a] by optimizing the adduct geometries (B3LYP-D3/TZ2P employing scalar relativistic corrections in calculations including Xe or I) and subjecting the resulting structures to an EDA according to the Morokuma-Ziegler scheme as summarized by Bickelhaupt and Baerends.[30] Adducts were separated in closed-shell components. The obtained orbital interaction was further decomposed in the frame of an Extended Transition State-Natural Orbitals for Chemical Valence (ETS-NOCV)[13a,31] approach yielding NOCVs connecting the two molecular fragments along with deformation densities visualizing source and destination regions of electron density that constitutes the respective NOCV.

Acknowledgements

K.R.A. acknowledges instrumental support from the Fritz-Haber-Institute of the Max-Planck Society. J.W. is grateful to the Volkswagen Foundation for a Freigeist-Fellowship. The computations for this work were done with resources of Leipzig University Computing Centre (M.R., M.M., H.K., S.K.). Open access funding enabled and organized by Projekt DEAL.

Conflict of Interest

The authors declare no conflict of interest.

Keywords: boron · electrophilic anions · IRPD spectroscopy · mass spectrometry · π-backbonding

[1] a) A. Li, F. P. Jjunju, R. G. Cooks, *J. Am. Soc. Mass Spectrom.* **2013**, *24*, 1745–1754; b) A. Patzer, S. Chakraborty, N. Solcà, O. Dopfer, *Angew. Chem. Int. Ed.* **2010**, *49*, 10145–10148; ; c) A. Patzer, S. Chakraborty, N. Solcà, O. Dopfer, *Angew. Chem.* **2010**, *122*, 10343–10346; ; d) J. Roithová, *Pure Appl. Chem.* **2011**, *83*, 1499–1506; e) D. Kuck, *Angew. Chem. Int. Ed.* **2010**, *49*, 4705–4706; ; f) D. Kuck, *Angew. Chem.* **2010**, *122*, 4813–4814; *Angew. Chem. Int. Ed.* **2010**, *49*, 4705–4706.

[2] a) J. Warneke, M. Mayer, M. Rohdenburg, X. Ma, J. K. Y. Liu, M. Grellmann, S. Debnath, V. A. Azov, E. Apra, R. P. Young, C. Jenne, G. E. Johnson, H. I. Kenttämaa, K. R. Asmis, J. Laskin, *Proc. Natl. Acad. Sci. USA* **2020**, *117*, 23374–23379; b) J. Laskin, G. E. Johnson, J. Warneke, V. Prabhakaran, *Angew. Chem. Int. Ed.* **2018**, *57*, 16270–16284; ; c) J. Laskin, G. E. Johnson, J. Warneke, V. Prabhakaran, *Angew. Chem.* **2018**, *130*, 16506–16521; .

[3] a) M. Mayer, V. van Lessen, M. Rohdenburg, G.-L. Hou, Z. Yang, R. M. Exner, E. Aprà, V. A. Azov, S. Grabowsky, S. S. Xantheas, K. R. Asmis, X.-B. Wang, C. Jenne, J. Warneke, *Proc. Natl. Acad. Sci. USA* **2019**, *116*, 8167–8172; b) M. Rohdenburg, M. Mayer, M. Grellmann, C. Jenne, T. Borrmann, F. Kleemiss, V. A. Azov, K. R. Asmis, S. Grabowsky, J. Warneke, *Angew. Chem. Int. Ed.* **2017**, *56*, 7980–7985; ; c) M. Rohdenburg, M. Mayer, M. Grellmann, C. Jenne, T. Borrmann, F. Kleemiss, V. A. Azov, K. R. Asmis, S. Grabowsky, J. Warneke, *Angew. Chem.* **2017**, *129*, 8090–8096; .

[4] A. Fielicke, G. von Helden, G. Meijer, D. B. Pedersen, B. Simard, D. M. Rayner, *J. Chem. Phys.* **2006**, *124*, 194305.

[5] M. Mayer, M. Rohdenburg, V. van Lessen, M. C. Nierstenhöfer, E. Aprà, S. Grabowsky, K. R. Asmis, C. Jenne, J. Warneke, *Chem. Commun.* **2020**, *56*, 4591–4594.

[6] a) A. J. Lupinetti, S. Fau, G. Frenking, S. H. Strauss, *J. Phys. Chem. A* **1997**, *101*, 9551–9559; b) A. S. Goldman, K. Krogh-Jespersen, *J. Am. Chem. Soc.* **1996**, *118*, 12159–12166.

[7] a) A. W. Mantz, J.-P. Maillard, W. B. Roh, K. Narahari Rao, *J. Mol. Spectrosc.* **1975**, *57*, 155–159; b) J. Bendtsen, *J. Raman Spectrosc.* **1974**, *2*, 133–145.

[8] a) L. Weber, *Angew. Chem. Int. Ed.* **1994**, *33*, 1077–1078; *Angew. Chem.* **1994**, *106*, 1131–1133; b) B. Liang, L. Andrews, *J. Phys. Chem. A* **2000**, *104*, 9156–9164; c) H. V. R. Dias, C. Dash, M. Yousufuddin, M. A. Celik, G. Frenking, *Inorg. Chem.* **2011**, *50*, 4253–4255; d) C. Dash, P. Kroll, M. Yousufuddin, H. V. R. Dias, *Chem. Commun.* **2011**, *47*, 4478–4480.

[9] a) T. A. Albright, J. K. Burdett, M.-H. Whangbo, *Orbital Interactions in Chemistry;* Wiley & Sons Ltd **2013**; b) P. K. Hurlburt, J. J. Rack, J. S. Luck, S. F. Dec, J. D. Webb, O. P. Anderson, S. H. Strauss, *J. Am. Chem. Soc.* **1994**, *116*, 10003–10014.

[10] G. Bistoni, S. Rampino, N. Scafuri, G. Ciancaleoni, D. Zuccaccia, L. Belpassi, F. Tarantelli, *Chem. Sci.* **2016**, *7*, 1174–1184.

[11] a) A. Fielicke, G. von Helden, G. Meijer, D. B. Pedersen, B. Simard, D. M. Rayner, *J. Am. Chem. Soc.* **2005**, *127*, 8416–8423; b) A. Fielicke, P. Gruene, G. Meijer, D. M. Rayner, *Surf. Sci.* **2009**, *603*, 1427–1433; c) A. Fielicke, G. von Helden, G. Meijer, B. Simard, S. Dénommée, D. M. Rayner, *J. Am. Chem. Soc.* **2003**, *125*, 11184–11185.

[12] M. Winkler, W. Sander, *J. Org. Chem.* **2006**, *71*, 6357–6367.

[13] a) M. P. Mitoraj, A. Michalak, T. Ziegler, *J. Chem. Theory Comput.* **2009**, *5*, 962–975; b) M. von Hopffgarten, G. Frenking, *WIREs Comput. Mol. Sci.* **2012**, *2*, 43–62.

[14] G. te Velde, F. M. Bickelhaupt, E. J. Baerends, C. Fonseca Guerra, S. J. A. van Gisbergen, J. G. Snijders, T. Ziegler, *J. Comput. Chem.* **2001**, *22*, 931–967.

[15] J. Warneke, G.-L. Hou, E. Aprà, C. Jenne, Z. Yang, Z. Qin, K. Kowalski, X.-B. Wang, S. S. Xantheas, *J. Am. Chem. Soc.* **2017**, *139*, 14749–14756.

[16] X. Wu, L. Zhao, J. Jin, S. Pan, W. Li, X. Jin, G. Wang, M. Zhou, G. Frenking, *Science* **2018**, *361*, 912–916.

[17] a) H. Braunschweig, I. Krummenacher, M.-A. Légaré, A. Matler, K. Radacki, Q. Ye, *J. Am. Chem. Soc.* **2017**, *139*, 1802–1805; b) H. Braunschweig, R. D. Dewhurst, F. Hupp, M. Nutz, K. Radacki, C. W. Tate, A. Vargas, Q. Ye, *Nature* **2015**, *522*, 327–330.
[18] a) N. Heine, K. R. Asmis, *Int. Rev. Phys. Chem.* **2015**, *34*, 1–34; b) N. Heine, K. R. Asmis, *Int. Rev. Phys. Chem.* **2016**, *35*, 507.
[19] a) I. Tiritiris, T. Schleid, *Z. Anorg. Allg. Chem.* **2004**, *630*, 1555–1563; b) V. Geis, K. Guttsche, C. Knapp, H. Scherer, R. Uzun, *Dalton Trans.* **2009**, 2687–2694; c) W. H. Knoth, H. C. Miller, J. C. Sauer, J. H. Balthis, Y. T. Chia, E. L. Muetterties, *Inorg. Chem.* **1964**, *3*, 159–167; d) D. V. Peryshkov, A. A. Popov, S. H. Strauss, *J. Am. Chem. Soc.* **2009**, *131*, 18393–18403.
[20] a) M. Brümmer, C. Kaposta, G. Santambrogio, K. R. Asmis, *J. Chem. Phys.* **2003**, *119*, 12700–12703; b) D. J. Goebbert, T. Wende, R. Bergmann, G. Meijer, K. R. Asmis, *J. Phys. Chem. A* **2009**, *113*, 5874–5880.
[21] N. Heine, *Vibrational spectroscopy of gaseous hydrogen-bonded clusters: On the role of isomer-specicity and anharmonicity*; Doctoral Thesis, Freie Universität Berlin, Berlin **2014**.
[22] W. R. Bosenberg, D. R. Guyer, *J. Opt. Soc. Am. B* **1993**, *10*, 1716.
[23] A. E. Reed, R. B. Weinstock, F. Weinhold, *J. Chem. Phys.* **1985**, *83*, 735–746.
[24] *Gaussian 09, revision D.01*, M. J. Frisch, G. W. Trucks, H. B. Schlegel, G. E. Scuseria, M. A. Robb, J. R. Cheeseman, G. Scalmani, V. Barone, G. A. Petersson, H. Nakatsuji, X. Li, M. Caricato, A. Marenich, J. Bloino, B. G. Janesko, R. Gomperts, B. Mennucci, H. P. Hratchian, J. V. Ortiz, A. F. Izmaylov, J. L. Sonnenberg, D. Williams-Young, F. Ding, F. Lipparini, F. Egidi, J. Goings, B. Peng, A. Petrone, T. Henderson, D. Ranasinghe, V. G. Zakrzewski, J. Gao, N. Rega, G. Zheng, W. Liang, M. Hada, M. Ehara, K. Toyota, R. Fukuda, J. Hasegawa, M. Ishida, T. Nakajima, Y. Honda, O. Kitao, H. Nakai, T. Vreven, K. Throssell, J. A. Montgomery, Jr, J. E. Peralta, F. Ogliaro, M. Bearpark, J. J. Heyd, E. Brothers, K. N. Kudin, V. N. Staroverov, T. Keith, R. Kobayashi, J. Normand, K. Raghavachari, A. Rendell, J. C. Burant, S. S. Iyengar, J. Tomasi, M. Cossi, J. M. Millam, M. Klene, C. Adamo, R. Cammi, J. W. Ochterski, R. L. Martin, K. Morokuma, O. Farkas, J. B. Foresman, and D. J. Fox, Gaussian, Inc, Wallingford CT **2013**.
[25] *Gaussian 16, revision C.01*, M. J. Frisch, G. W. Trucks, H. B. Schlegel, G. E. Scuseria, M. A. Robb, J. R. Cheeseman, G. Scalmani, V. Barone, G. A. Petersson, H. Nakatsuji, X. Li, M. Caricato, A. V. Marenich, J. Bloino, B. G. Janesko, R. Gomperts, B. Mennucci, H. P. Hratchian, J. V. Ortiz, A. F. Izmaylov, J. L. Sonnenberg, D. Williams-Young, F. Ding, F. Lipparini, F. Egidi, J. Goings, B. Peng, A. Petrone, T. Henderson, D. Ranasinghe, V. G. Zakrzewski, J. Gao, N. Rega, G. Zheng, W. Liang, M. Hada, M. Ehara, K. Toyota, R. Fukuda, J. Hasegawa, M. Ishida, T. Nakajima, Y. Honda, O. Kitao, H. Nakai, T. Vreven, K. Throssell, Montgomery, J. A, Jr, J. E. Peralta, F. Ogliaro, M. J. Bearpark, J. J. Heyd, E. N. Brothers, K. N. Kudin, V. N. Staroverov, T. A. Keith, R. Kobayashi, J. Normand, K. Raghavachari, A. P. Rendell, J. C. Burant, S. S. Iyengar, J. Tomasi, M. Cossi, J. M. Millam, M. Klene, C. Adamo, R. Cammi, J. W. Ochterski, R. L. Martin, K. Morokuma, O. Farkas, J. B. Foresman, D. J. Fox, Gaussian, Inc, Wallingford CT **2016**.
[26] A. D. Becke, *J. Chem. Phys.* **1993**, *98*, 5648–5652.
[27] a) F. Weigend, *Phys. Chem. Chem. Phys.* **2006**, *8*, 1057–1065; b) F. Weigend, R. Ahlrichs, *Phys. Chem. Chem. Phys.* **2005**, *7*, 3297–3305.
[28] S. Grimme, S. Ehrlich, L. Goerigk, *J. Comput. Chem.* **2011**, *32*, 1456–1465.
[29] a) S. F. Boys, F. Bernardi, *Mol. Phys.* **1970**, *19*, 553–566; b) S. Simon, M. Duran, J. J. Dannenberg, *J. Chem. Phys.* **1996**, *105*, 11024–11031.
[30] a) F. M. Bickelhaupt, E. J. Baerends, *Reviews in Computational Chemistry*, Vol. 15 (Eds.: K. B. Lipkowitz, D. B. Boyd), Wiley-VCH, Weinheim, 2000, pp. 1–86; **2000**; b) T. Ziegler, A. Rauk, *Theor. Chim. Acta* **1977**, *46*, 1–10; c) K. Kitaura, K. Morokuma, *Int. J. Quantum Chem.* **1976**, *10*, 325–340.
[31] M. P. Mitoraj, A. Michalak, T. Ziegler, *Organometallics* **2009**, *28*, 3727–3733.

Manuscript received: March 15, 2021
Accepted manuscript online: May 20, 2021
Version of record online: June 17, 2021

